Robust Error-State Kalman Filter for Estimating IMU Orientation

Rachel V. Vitali, Ryan S. McGinnis, *Member, IEEE*, and Noel C. Perkins

***Abstract*—Inertial measurement units (IMUs) are increasingly utilized as motion capture devices in human movement studies. Given their high portability, IMUs can be deployed in any environment, importantly those outside of the laboratory. However, a significant challenge limits the adoption of this technology; namely estimating the orientation of the IMUs to a common world frame, which is essential to estimating the rotations across skeletal joints. Common (probabilistic) methods for estimating IMU orientation rely on the ability to update the current orientation estimate using data provided by the IMU. The objective of this work is to present a novel error-state Kalman filter that yields highly accurate estimates of IMU orientation that are robust to poor measurement updates from fluctuations in the local magnetic field and/or highly dynamic movements. The method is validated with ground truth data collected with highly accurate orientation measurements provided by a coordinate measurement machine. As an example, the method yields IMU-estimated orientations that remain within 3.7 degrees (RMS error) over relatively long (25 cumulative minutes) trials even in the presence of large fluctuations in the local magnetic field. For comparison, ignoring the magnetic interference increases the RMS error to 12.8 degrees, more than a threefold increase.**

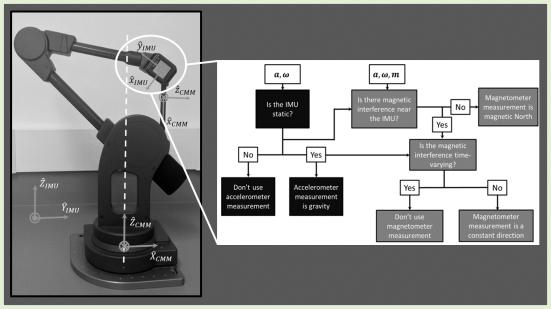

***Index Terms*—Inertial measurement unit, IMU, indirect Kalman filtering, orientation estimation.**

I. Introduction

INERTIAL measurement units (IMUs) are highly portable motion capture devices supporting human movement studies in any environment including those outside of a laboratory. Unlike optical motion capture, inertial motion capture is not restricted to relatively small (lab-based) capture volumes and can therefore be deployed in natural settings such as the clinic, home, workplace, and training environment. Thus, inertial motion capture is a promising technology for understanding human movement and performance in broad contexts, which frequently begins by estimating the orientation of an IMU in space. For instance, estimating the angles across the major skeletal joints (a common need in biomechanical analyses) first requires knowing the orientation of the IMUs attached to the adjacent body segments [1].

Approaches for estimating IMU orientation typically fuse independent orientation estimates from acceleration, angular rate, and (possibly) magnetometer data. The methods fall into two broad categories, namely: 1) deterministic (complementary) and 2) probabilistic (stochastic) methods. Bachmann *et al.* [2] and Mahony *et al.* [3] propose complementary filter algorithms that rely on accelerometer-derived estimates of orientation during low dynamic periods while relying on angular rate gyro-derived estimates of orientation during high dynamic periods. These two studies laid the foundation for the most well known deterministic approach, Madgwick's filter [4], which yields orientation estimates that tend to lag the true state during sustained highly dynamic movements [5]. However, recent efforts have shown specific design choices, like tunable gains and employing a rotation vector parameterization of orientation deviation, can significantly improve performance [6]–[8]. Generally, complementary filters tend to be computationally efficient, making them ideal for real-time estimation for a number of applications like exoskeleton control [9], robot teleoperation [10], and dynamic balance biofeedback [11].

Probabilistic approaches, most often employing indirect Kalman filtering, have opposite strengths and weaknesses; they tend to be more computationally expensive [12], but yield accurate orientation estimates even during prolonged

Manuscript received September 1, 2020; accepted September 22, 2020. Date of publication September 25, 2020; date of current version January 6, 2021. This work was supported by the U.S. Army Contracting Command-APG, Natick Contracting Division, Natick, MA, USA, under Contract W911QY-15-C-0053. The work of Ryan S. McGinnis was supported by the MC10, Inc., and Impellia. The associate editor coordinating the review of this article and approving it for publication was Dr. You Li. *(Corresponding author: Rachel V. Vitali.)*

Rachel V. Vitali is with the Department of Mechanical Engineering, The University of Iowa, Iowa City, IA 52242 USA (e-mail: rvitali@uiowa.edu).

Ryan S. McGinnis is with the Department of Electrical and Biomedical Engineering, University of Vermont, Burlington, VT 05405 USA (e-mail: ryan.mcginnis@uvm.edu).

Noel C. Perkins is with the Department of Mechanical Engineering, University of Michigan, Ann Arbor, MI 48109 USA (e-mail: ncp@umich.edu).

Digital Object Identifier 10.1109/JSEN.2020.3026895

dynamic movements (provided the filter is parameterized properly) [5]. The probabilistic formulations achieve more accurate orientation estimates by leveraging additional information (e.g., magnetometer data [13] or biomechanical kinematic constraints [1]), but inappropriate measurement updates (even once) can cause the estimates to diverge [14]. The Kalman filter is the optimal estimator that minimizes the mean squared error when the state and measurement dynamics are modeled as linear and the process/measurement noise processes are modeled as white Gaussian [15]. While the equations governing orientation estimates are nonlinear, successful implementations exist. Noteworthy examples of state-of-the-art implementations include the Particle filter [16], [17], the Extended Kalman filter (EKF) [18], [19], the Sigma-Point (Unscented) Kalman filter [20], [21], the Invariant Extended Kalman filter [22], [23], and the Error-State Kalman filter (ESKF) [15], [24], [25], the last of which is central to this work.

The key idea underlying the error-state formulation of the Kalman filter is to decompose the true state of the system (i.e., quaternion representation of the IMU's orientation) into a nominal-state and an error-state [24]. The nominal-state arises from integrating the IMU data without consideration of noise or model imperfections. Then, errors resulting from that integration are attributed to the error-state, whose dynamic equations are *linear* with respect to the error-state. The benefits of the ESKF formulation are outlined by Madyastha *et al.* [15] and Solà [25] and briefly summarized here. The orientation error-state is a minimal parameterization because the scalar term of the quaternion (q_0) is unity since the error in orientation is assumed small (i.e., $cos(\theta) \approx 1$ when θ is small). This approximation avoids singularities in the covariance matrices arising from enforced constraints (i.e., forcing the quaternions to have unit magnitudes). Next, the error-state is assumed small such that linearization remains accurate. Finally, the error state dynamics are relatively slow compared to those of the (deterministic) nominal-state, which means corrections to the error-state can be made less frequently than in an EKF. Consequently, the criteria for integrating measurements into the state estimation can be stricter to avoid divergence. Thus, the challenge then becomes developing those criteria to provide sufficient opportunities to correct for inevitable integration drift error.

Consequently, external disturbances must be carefully considered to render the method robust by avoiding irreparable divergence in the orientation estimates. For example, an estimate of magnetic North can be integrated into the method using magnetometer data to correct orientation about vertical [13]. However, magnetometer data is often polluted by surrounding ferromagnetic materials in the local environment (e.g., equipment, building materials, and wiring) thereby yielding faulty estimates of magnetic North [26]. Prolonged exposure to magnetic interference (as is frequently the case indoors) or prolonged highly dynamic movement (as is frequently the case with in biomechanical studies) renders IMU orientation estimation a difficult challenge over long periods of time, especially when updating current estimates with other data sources. This challenge is further confounded by differing hardware characteristics.

Researchers have proposed many distinct approaches to minimize the errors introduced by inappropriately incorporating accelerometer and/or magnetometer data. For accelerometer data, Sabatini [18] proposed simple thresholding criteria for measured acceleration magnitude to determine whether the accelerometer was reliably acting as an inclinometer update the current orientation estimates relative to the horizontal plane (e.g., pitch and roll). Similarly, Xu *et al.* [27] also use simple thresholding for the measured angular velocity, measured acceleration, calculated jerk, and mean estimated innovation to determine which data are reliable for propagation and updating. Further, Xu *et al.* [28] use simple thresholding for the measured acceleration magnitude and direction when compared to the expected magnitude and direction of gravity to evaluate the reliability of the accelerometer. Kang and Park [29] use fuzzy logic to adapt the measurement noise of the accelerometer depending on the magnitude of the measured acceleration and angular velocity.

For magnetometer data, Sabatini [18] and Yadav and Bleakley [16] propose simple thresholding criteria for measured magnetic field magnitude and inclination angle to determine whether the magnetometer can reliably update the current orientation estimate about the vertical axis (e.g., yaw). Similarly, Xu *et al.* [28] use simple thresholding for the measured magnetic field magnitude and direction when compared to the expected magnitude and direction of magnetic North to evaluate the reliability of the magnetometer. Roetenberg *et al.* [30] modeled magnetic disturbance as a Markov process driven by Gaussian noise parameterized by the magnitude and inclination angle of the measured magnetic field to compensate for any interference. In their latest generational IMU design and accompanying proprietary software, Xsens conducts magnetic field mapping whereby local magnetic disturbances are mapped and removed via localization by exploiting the unique signatures of those local magnetic disturbances [31], [32]. Wu [33] estimates magnetic disturbances in real-time with a nonlinear optimization that exploits the current orientation estimation derived from the angular rate gyroscope and accelerometer.

The objective of this work is to present an ESKF method for estimating IMU orientation that is robust and adaptable for human movement studies. The method's success arises from frequently and appropriately updating current estimates derived from angular rate gyro data with accelerometer and magnetometer data. The proposed method is physically intuitive, probabilistically inferential, and adaptable such that it can be tailored to any IMUs (i.e., IMUs with different sensor characteristics) or testing conditions (i.e., subject-specific criteria). The effectiveness of the method is demonstrated and evaluated for a single IMU in challenging testing conditions, for which a novel treatment of magnetometer data is also introduced. The orientation estimates are validated using highly accurate (ground truth) measurements provided by a coordinate measurement machine (CMM). This experimental design, employing a CMM, controls for other confounding sources of error that would otherwise be present on human subjects

(e.g., soft-tissue artifacts and anatomical frame definition). Nonetheless, the method has significant promise for human movement studies.

II. Methods

A. ESKF Process Model and Propagation Step

The method herein draws largely from [15] and [25], starting with the continuous (nonlinear) dynamical equations for the quaternion, $\boldsymbol{q}$, describing the orientation of the IMU, and the angular rate gyro biases, $\boldsymbol{\omega}_b$, representing the slowly varying dc offsets in the angular velocity measurements

$$\dot{\hat{\boldsymbol{x}}}(t) = \begin{bmatrix} \dot{\hat{\boldsymbol{q}}}(t) \\ \dot{\hat{\boldsymbol{\omega}}}_b(t) \end{bmatrix} = \begin{bmatrix} \frac{1}{2}\boldsymbol{q}(t) \otimes (\boldsymbol{\omega}(t) - \boldsymbol{\omega}_b(t) - \tilde{\boldsymbol{\omega}}_n) \\ \tilde{\boldsymbol{\omega}}_w \end{bmatrix} \quad (1)$$

Here $\otimes$ represents the quaternion product, $\tilde{\boldsymbol{\omega}}_n$ is the measurement noise in the angular rate gyro, and $\tilde{\boldsymbol{\omega}}_w$ is the process noise in the angular rate gyro bias estimate (modeled as a zero-mean random walk). The ESKF defines the true state of the system, $\boldsymbol{x}_t$, as the sum of the nominal-state, $\boldsymbol{x}_n$, and the error-state, $\boldsymbol{\delta x}$. The nominal-state is governed by Eqn. 1 while ignoring the process noise. The error-state dynamics describe a small perturbation, $\boldsymbol{\delta x}$, from the nominal-state. Accordingly, $\boldsymbol{\delta x}$ is governed by a first-order Taylor series expansion of Eqn. 1 about $\boldsymbol{x}$ (and adding the appropriate process noise) per the following continuous error-state process model

$$\boldsymbol{\delta x}(t) = \begin{bmatrix} \boldsymbol{\delta\theta}(t) \\ \boldsymbol{\delta\omega}_b(t) \end{bmatrix} = \begin{bmatrix} -\boldsymbol{u}(t)^{\times}\boldsymbol{\delta\theta}(t) - \boldsymbol{\delta\omega}_b(t) - \tilde{\boldsymbol{\omega}}_n \\ \tilde{\boldsymbol{\omega}}_w \end{bmatrix} \quad (2)$$

where $\boldsymbol{u} = \boldsymbol{\omega}_m - \boldsymbol{\omega}_b$, $\boldsymbol{\delta\theta}$ is the quaternion angle error, $\boldsymbol{\delta\omega}_b$ is the angular rate gyro bias error, $\tilde{\boldsymbol{\omega}}_n$ is the process noise associated with $\boldsymbol{\delta\theta}$, and $\tilde{\boldsymbol{\omega}}_w$ is the process noise associated with $\boldsymbol{\delta\omega}_b$. The quantity, $\boldsymbol{u}^{\times}$, denotes the skew symmetric form of the vector. Discretizing the error-state process model for time steps δt yields

$$\boldsymbol{\delta x}_k = \begin{bmatrix} \boldsymbol{R}\{\boldsymbol{u}_k \Delta t\}^T & -\Delta t \boldsymbol{I} \\ \boldsymbol{0} & \boldsymbol{I} \end{bmatrix} \begin{bmatrix} \boldsymbol{\delta\theta}_k \\ \boldsymbol{\delta\omega}_{b,k} \end{bmatrix} + \begin{bmatrix} \boldsymbol{\theta}_{i,k} \\ \boldsymbol{\omega}_{i,k} \end{bmatrix} \quad (3)$$

where $\boldsymbol{\theta}_{i,k}$ and $\boldsymbol{\omega}_{i,k}$ are random impulses applied to the orientation and angular rate gyro bias estimates modeled by the Gaussian processes $\tilde{\boldsymbol{\omega}}_n$ and $\boldsymbol{\delta\omega}_b$. The error covariance matrix, $\hat{\boldsymbol{P}}$, is propagated per

$$\hat{\boldsymbol{P}}_k = \boldsymbol{F}\hat{\boldsymbol{P}}_{k-1}\boldsymbol{F}^T + \boldsymbol{Q} \quad (4)$$

where $\boldsymbol{F}$ is the state transition matrix from Eqn. 3 and $\boldsymbol{Q}$ is the process noise matrix associated with the random impulses in Eqn. 3. For a thorough derivation of this result, see [25].

B. ESKF Measurement Models and Update Step

First, the measurement model for the accelerometer is

$$\hat{\boldsymbol{y}}_{a,k} = \boldsymbol{R}\{\hat{\boldsymbol{q}}_k\}\hat{\boldsymbol{g}} + \tilde{\boldsymbol{a}}_n \quad (5)$$

where $\boldsymbol{R}\{\hat{\boldsymbol{q}}\}$ is the direction cosine matrix representing the orientation of the IMU relative to a world frame, $\hat{\boldsymbol{g}}$ is the expected, measured direction of gravity, and $\tilde{\boldsymbol{a}}_n$ is the accelerometer measurement noise. The expected, measured direction of gravity (resolved in the world frame) is aligned with the vertical axis in the positive direction (e.g., $\hat{\boldsymbol{g}} = [0, 0, 1]^T$). Similarly, the measurement model for the magnetometer is

$$\hat{\boldsymbol{y}}_{m,k} = \boldsymbol{R}\{\hat{\boldsymbol{q}}_k\}\hat{\boldsymbol{b}} + \tilde{\boldsymbol{m}}_n \quad (6)$$

where $\hat{\boldsymbol{b}}$ is the expected, measured direction of the magnetic field and $\tilde{\boldsymbol{m}}_n$ is the magnetometer noise. The expected, measured direction of the magnetic field is magnetic North (e.g., $\hat{\boldsymbol{b}} = [1, 0, 0]^T$). The innovation, $\mathcal{I}$, between the actual measurements and the estimated measurements becomes

$$\mathcal{I}_k = \boldsymbol{y}_k - \hat{\boldsymbol{y}}_k = \begin{bmatrix} \boldsymbol{y}_{a,k} - \hat{\boldsymbol{y}}_{a,k} \\ \boldsymbol{y}_{m,k} - \hat{\boldsymbol{y}}_{m,k} \end{bmatrix} = \begin{bmatrix} \boldsymbol{a}_{m,k} - \boldsymbol{R}\{\hat{\boldsymbol{q}}_k\}\hat{\boldsymbol{g}} \\ \boldsymbol{m}_{m,k} - \boldsymbol{R}\{\hat{\boldsymbol{q}}_k\}\hat{\boldsymbol{b}} \end{bmatrix} \quad (7)$$

where $\boldsymbol{a}_{m,k}$ is the normalized accelerometer measurement and $\boldsymbol{m}_{m,k}$ is the normalized magnetometer measurement. The uncertainty associated with the innovation, $\boldsymbol{S}$, is defined as

$$\boldsymbol{S}_k = \boldsymbol{H}_{\delta x,k}\hat{\boldsymbol{P}}_k^{-}\boldsymbol{H}_{\delta x,k}{}^T + \boldsymbol{R} \quad (8)$$

where $\hat{\boldsymbol{P}}_k^{-}$ is the propagated (*a priori*) error covariance matrix (i.e., $\hat{\boldsymbol{P}}_k$ from Eqn. 4), $\boldsymbol{R}$ is the measurement noise, and $\boldsymbol{H}_{\delta x}$ is the Jacobian of the measurement models given by

$$\begin{aligned} \boldsymbol{H}_{\delta x} &= \frac{\partial}{\partial \hat{\boldsymbol{\delta x}}} h(\hat{\boldsymbol{x}}) \\ &= \frac{\partial}{\partial \hat{\boldsymbol{x}}} h(\hat{\boldsymbol{x}}) \frac{\partial \hat{\boldsymbol{x}}}{\partial \hat{\boldsymbol{\delta x}}} \\ &= \boldsymbol{H}\boldsymbol{X}_{\delta x} \end{aligned} \quad (9)$$

where

$$\boldsymbol{H} = 2\begin{bmatrix} q_0\hat{\boldsymbol{g}} + \hat{\boldsymbol{g}} \times \boldsymbol{p} & \boldsymbol{p}^T\hat{\boldsymbol{g}}\boldsymbol{I} + \boldsymbol{p}\hat{\boldsymbol{g}}^T - \hat{\boldsymbol{g}}\boldsymbol{p}^T + q_0\hat{\boldsymbol{g}}^{\times} \\ q_0\hat{\boldsymbol{b}} + \hat{\boldsymbol{b}} \times \boldsymbol{p} & \boldsymbol{p}^T\hat{\boldsymbol{b}}\boldsymbol{I} + \boldsymbol{p}\hat{\boldsymbol{b}}^T - \hat{\boldsymbol{b}}\boldsymbol{p}^T + q_0\hat{\boldsymbol{b}}^{\times} \end{bmatrix} \quad (10)$$

$$\boldsymbol{X}_{\delta x} = \begin{bmatrix} \boldsymbol{Q}_{\delta x} & \boldsymbol{0} \\ \boldsymbol{0} & \boldsymbol{I} \end{bmatrix} \quad (11)$$

$$\boldsymbol{Q}_{\delta x} = \frac{1}{2}\begin{bmatrix} -q_1 & -q_2 & -q_3 \\ q_0 & -q_3 & q_2 \\ q_3 & q_0 & -q_1 \\ -q_2 & q_1 & q_0 \end{bmatrix} \quad (12)$$

Here, q_0 denotes the scalar component of the quaternion while $\boldsymbol{p}$ denotes the vector component of the quaternion (q_1, q_2, q_3). For a thorough derivation of this result, see [34]. The Kalman filter gain is therefore

$$\boldsymbol{K}_k = \hat{\boldsymbol{P}}_k^{-}\boldsymbol{H}_{\delta x,k}{}^T\boldsymbol{S}_k{}^{-1} \quad (13)$$

which is used to scale the correction provided by the innovation by taking into account the uncertainty associated with both the estimated state and the measurements themselves per

$$\Delta\hat{\boldsymbol{x}}_k = \boldsymbol{K}_k\mathcal{I}_k \quad (14)$$

which is incorporated into the current estimate. The (*a posteriori*) error covariance matrix, $\hat{\boldsymbol{P}}_k^{+}$, is likewise updated per

$$\hat{\boldsymbol{P}}_k^{+} = (\boldsymbol{I} - \boldsymbol{K}_k\boldsymbol{H}_k)\hat{\boldsymbol{P}}_k^{-} \quad (15)$$

where $\boldsymbol{I}$ is the identity matrix. For the full derivation of this result, see [25].

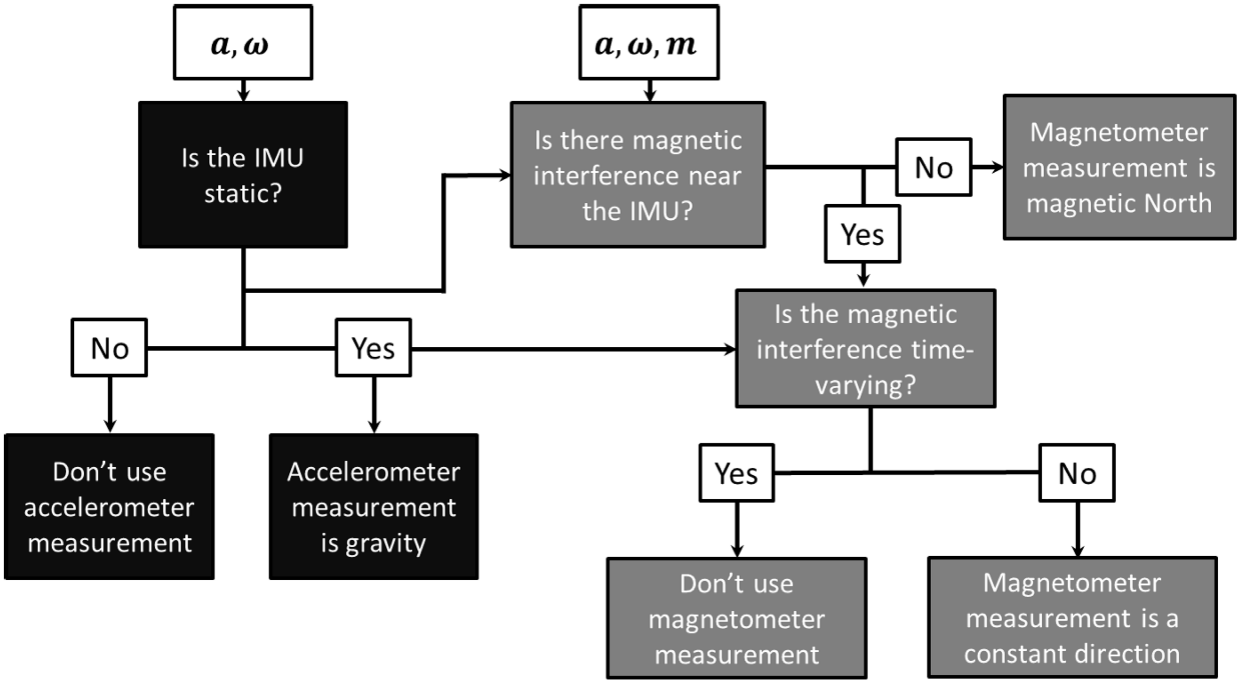

Fig. 1. Decision tree governing when to trust or not trust the additional measurements from the accelerometer and magnetometer.

C. Robust Decision Making Framework

To reiterate, inappropriately applying updates to the current estimate with the accelerometer and/or magnetometer data can cause the filter to diverge irreparably. For example, significant dynamics render the accelerometer a very poor inclinometer leading to large deviations of estimated gravity from vertical. Also, any perturbation to the local magnetic field can lead to very large deviations of the magnetic field lines from magnetic North. This section describes the major contribution of this work, namely the methodology illustrated by the decision tree shown in Fig. 1 to render the filter robust to inappropriate updates. Note that the decision tree excludes the case when the IMU is not static and magnetic interference is also detected. During human movement, it is improbable for an IMU attached to a body segment to be solely rotating (i.e., possess no translation). The body segment (including the attached IMU) will be moving relative to the source of the magnetometer interference, thereby producing a time-varying interference. More complex approaches can compensate for dynamic magnetic interference (see, for example, [33]).

In Fig. 1, the black boxes pertain to decisions concerning the accelerometer data and the grey boxes relate to decisions concerning the magnetometer data. The decision tree starts by determining whether the IMU is static using the acceleration and angular velocity data. If the IMU is static, then the accelerometer measurement yields a valid estimate of the direction of gravity (i.e., the accelerometer functions as an inclinometer). If the IMU is not static, then the accelerometer measurement is polluted by the additional acceleration experienced by the rigid body to which the IMU is attached (i.e., the accelerometer becomes a poor inclinometer).

The decision tree continues by determining if there is magnetic interference near the IMU, which requires data (acceleration, angular velocity, and magnetic field) from all three on-board sensors. One criterion distinguishes if magnetic interference is present when the IMU is static and the second criterion distinguishes if that is the case when the IMU is not static. If no magnetic interference is detected, the magnetometer measurement yields a valid estimation of the direction of magnetic North. Beyond that, a third novel criterion is introduced. If magnetic interference is detected when the IMU is static, there is still an opportunity to use the magnetometer data by determining if the magnetic interference is largely constant versus time-varying. If it is largely constant, then the magnetometer is providing a constant measured direction, albeit not in the direction of magnetic North. In this instance, the magnetometer data still provides an opportunity to correct for local integration drift error about the vertical axis. In particular, the expected direction of the magnetic field is simply the direction during the previous time step (instead of magnetic North). The criteria pertaining to both the accelerometer and magnetometer are summarized as follows.

1) Accelerometer Criteria: The criteria for determining whether the IMU is static leverages the triangle inequality

$$\|\boldsymbol{x} + \boldsymbol{y}\| \leqslant \|\boldsymbol{x}\| + \|\boldsymbol{y}\| \tag{16}$$

where $\boldsymbol{x}$ and $\boldsymbol{y}$ are two vectors (with the same number of elements). Knowing that the accelerometer is measuring both the acceleration of the rigid body ($\boldsymbol{a}_{body}$) and the acceleration due to gravity ($\boldsymbol{g}$), Eqn. 16 yields

$$\left\|\boldsymbol{R}\boldsymbol{a}_{body} + \boldsymbol{g}\right\| \leqslant \left\|\boldsymbol{R}\boldsymbol{a}_{body}\right\| + \|\boldsymbol{g}\| \tag{17}$$

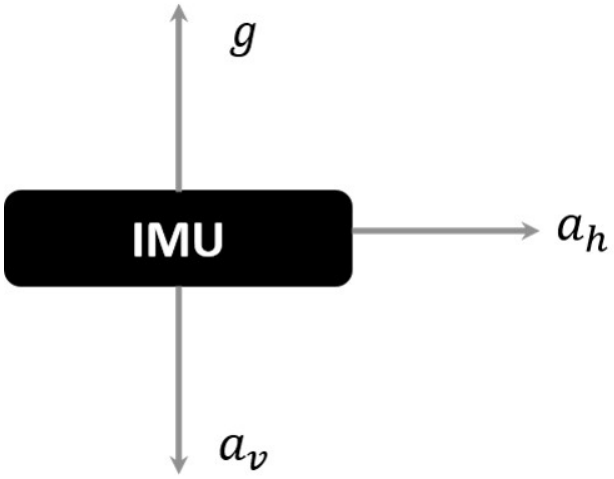

Fig. 2. An IMU illustrated with the measured direction of gravity, $\boldsymbol{g}$, and hypothetical rigid body vertical accelerations, $\boldsymbol{a_v}$, (parallel to and opposite gravity) and horizontal accelerations, $\boldsymbol{a_h}$ (perpendicular to gravity).

where $\boldsymbol{R}$ is the direction cosine matrix relating the IMU frame to the world frame. This can be further simplified to

$$\|\boldsymbol{a}_m\| \leqslant \|\boldsymbol{a}_{body}\| + \|\boldsymbol{g}\| \tag{18}$$

where $\boldsymbol{a}_m$ is the measured acceleration provided by the IMU and noting the magnitude of $\boldsymbol{a}_{body}$ is independent of reference frame. If the rigid body to which the IMU is attached is not accelerating ($\|\boldsymbol{a}_{body}\| = 0$), then the IMU is considered static and Eqn. 18 reduces to

$$\|\boldsymbol{a}_m\| = \|\boldsymbol{g}\| \tag{19}$$

This is relaxed slightly to account for measurement noise per Criterion 1A

$$\big|\, \|\boldsymbol{a}_m\| - \|\boldsymbol{g}\| \,\big| \leqslant \epsilon_a \tag{20}$$

for which [18] successfully uses a value of $\epsilon_a = 0.2\ m/s^2$. This criterion is tantamount to trusting that the accelerometer functions as an inclinometer. However, Eqn. 20 represents only one of two criteria needed to determine if the IMU is static (thus, if the accelerometer data can be used to estimate gravity).

There are other possibilities in which Eqn. 18 reduces to the equality Eqn. 19. Consider Fig. 2 in which the rigid body acceleration has components in the opposite direction of and also perpendicular to gravity; namely, the components $\boldsymbol{a_v}$ and $\boldsymbol{a_h}$, respectively. The magnitude of the measured acceleration of the IMU now becomes

$$\|\boldsymbol{a}_m\| = \sqrt{(\boldsymbol{g} - \boldsymbol{a_v})^2 + \boldsymbol{a_h}^2} \tag{21}$$

If the magnitude of the measured acceleration is assumed to be equal to gravity per Eqn. 19, then Eqn. 21 yields

$$\boldsymbol{a_v}(2\boldsymbol{g} - \boldsymbol{a_v}) = \boldsymbol{a_h}^2 \tag{22}$$

which admits *three* solutions. The first is the trivial solution (the vertical and horizontal components of the acceleration are zero), which replicates Criterion A1; namely Eqn. 19 and thus Eqn. 20. A second solution arises when the horizontal component is zero and the vertical component equals $2\boldsymbol{g}$. The third solution arises when $\boldsymbol{a_h} = \sqrt{2\boldsymbol{g}\boldsymbol{a_v} - \boldsymbol{a_v}^2}$ for $\boldsymbol{a_v} \in [0, 2\boldsymbol{g}]$ (note the sign of $\boldsymbol{a_v}$ flips when $\boldsymbol{a_v} > 2\boldsymbol{g}$ in which case the vertical acceleration aligns with measured gravity). Reflecting on the two nontrivial solutions, it is highly unlikely during human movement that these acceleration components will arise from purely linear acceleration; that is, some portion of the acceleration will also arise from the angular velocity as evidenced by nonzero measured angular rate. Thus, one must also simultaneously consider the measured angular rate. Therefore, a second criterion (Criterion A2) considers the magnitude of the angular velocity using the Mahalanobis distance [35]. The Mahalanobis distance, D, is the generalized distance from any sample to a distribution composed of n normally distributed variables per

$$D(x) = \sqrt{(\boldsymbol{x} - \boldsymbol{\mu})^T \boldsymbol{\Sigma}^{-1} (\boldsymbol{x} - \boldsymbol{\mu})} \tag{23}$$

where $\boldsymbol{x}$ denotes the sample, $\boldsymbol{\mu}$ is the mean of the distribution, and $\boldsymbol{\Sigma}$ is the covariance of the distribution. A χ^2 test with n degrees of freedom can be used to determine if an angular velocity sample is from the normal distribution characterized by data collected during a static period at the beginning of a trial [36]. However, the angular velocity magnitude distributions are necessarily positively skewed, which is remedied with a natural log transformation to yield

$$\boldsymbol{x} = ln(|\boldsymbol{\omega}_m|) \tag{24}$$

which is used with Eqn. 23 to form Criterion A2

$$D(ln(|\boldsymbol{\omega}_m|))^2 \leqslant \chi^2(1 - \alpha, n) \tag{25}$$

where α is the significance level and n is the degrees of freedom. Thus, when both Criterion A1 and Criterion A2 are met, the IMU is considered to be static.

2) Magnetometer Criteria: Determining whether there is magnetic interference present in the local environment of the IMU requires different criteria depending on if the IMU is static or not. If it is static, the angle between the accelerometer and magnetometer measurements is calculated per

$$\theta = \left| \cos^{-1}\left(\frac{\boldsymbol{m}_m \cdot \boldsymbol{a}_m}{\|\boldsymbol{m}_m\|\, \|\boldsymbol{a}_m\|} \right) \right| \tag{26}$$

which is then compared to a distribution characterized by data collected during a static period at the beginning of a trial via the squared Mahalanobis distance and a χ^2 test (similar to that of Eqn. 25) to form Criterion M1. It is assumed that magnetic interference is not present during the static period at the beginning of a trial. It is assumed that magnetic interference is not present during the static period at the beginning of a trial.

If the IMU is not static, then the yaw angular velocity is calculated from the magnetometer data and compared to that derived from the estimated state and measured angular velocity. The magnetometer-based yaw angular velocity magnitude ($\dot{\psi}_m$) is calculated via a simple numerical derivative per

$$\dot{\psi}_m = \left| \frac{1}{\Delta t} \cos^{-1}\left(\frac{m_k \cdot m_{k-1}}{\|m_k\|\, \|m_{k-1}\|} \right) \right| \tag{27}$$

The gyro-based yaw angular velocity magnitude ($\dot{\psi}_\omega$) is

$$\dot{\psi}_\omega = \left| -\frac{\sin(\phi)}{\cos(\theta)}\omega_y + \frac{\cos(\phi)}{\cos(\theta)}\omega_z \right| \tag{28}$$

where ϕ and θ are Euler angles representing the current estimated state and ω_y and ω_z are measured angular velocity components. Similar to Eqn. 20, Criterion M2 tests if the magnitude of the difference between these two estimated yaw rates is below some threshold, e.g.,

$$|\dot{\psi}_m - \dot{\psi}_\omega| \leqslant \epsilon_m \tag{29}$$

where $\epsilon_m = 10\,^\circ/s$, which is the RMS of the estimated angular velocity calculated from the (noisy) magnetometer data collected during a known static period. If it is determined that magnetic interference is not present, then the magnetometer measurement yields a reliable estimate of magnetic North and is used accordingly.

If magnetic interference is detected, the next step is to determine if the interference is constant versus time-varying. While the magnetic field around the IMU may vary spatially, it does not necessarily vary in time. If the IMU is static and the magnetic field is time-invariant, the magnetometer data yields an estimate of a *constant* direction (that may not be magnetic North). The constant direction can be used to correct for local drift error in orientation about the vertical axis (i.e., yaw drift). This is achieved by calculating the magnitude of the angular velocity of the IMU from the magnetometer measurements using Eqn. 27 and testing the squared Mahalanobis distance from that sample to the magnetometer-estimated angular velocity distribution characterized by the data collected during a static period (representing Criterion M3). If it is determined the magnetic field is not time-varying, the expected direction of the magnetic field is the magnetometer measurement from the previous time step. Specifically, the previous time step's normalized magnetometer measurement, $m_{m,k-1}$, is resolved in the world frame and becomes the expected, measured direction of the magnetic field, $\hat{\boldsymbol{b}}$, in Eqn. 6.

D. Experimental Procedure

To validate the accuracy of the above method for estimating the orientation of a single IMU, results from the orientation estimation method above are compared with truth data provided by the coordinate measurement machine (CMM) illustrated in Fig. 3. The IMU is a commercial design (APDM, Opal, Portland OR) with companion proprietary software that provides estimates of IMU orientation. The CMM provides highly accurate measures of three-dimensional rotations via embedded optical encoders. The encoders measure the three component angles of rotation to a 0.004° resolution.

Data from the IMU is first time-synchronized to the encoder data from the CMM as follows. The assembly is first oscillated clockwise and counterclockwise by hand about the vertical axis of the CMM's base for about 5 seconds while the other joints remain locked. We call this movement the alignment movement and during this movement the entire CMM reduces to a single rigid body. The angle measured by the optical encoder about the base axis during this alignment movement is

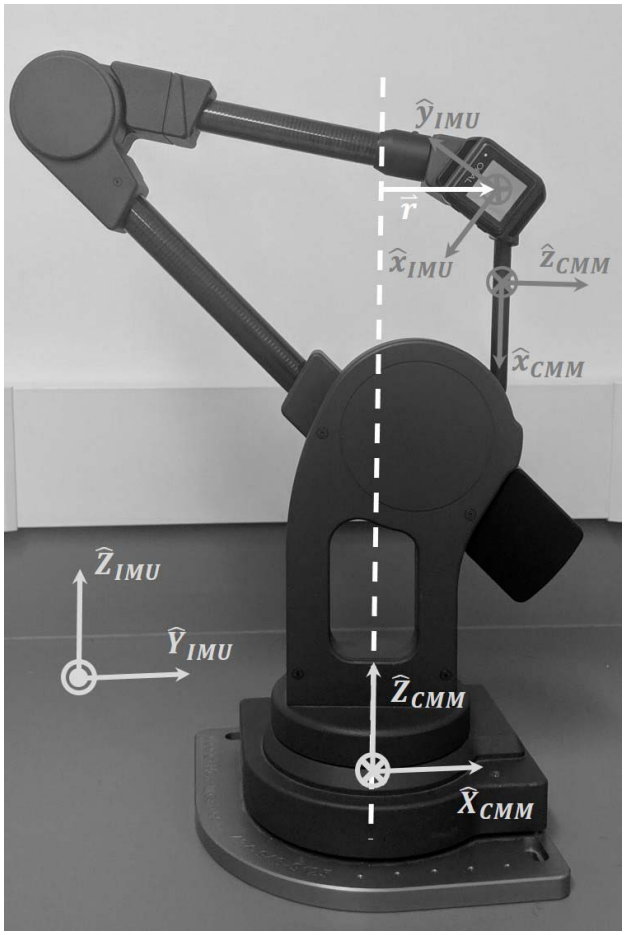

Fig. 3. Set-up for validation of IMU-estimated orientation with the IMU attached to the end effector of a coordinate measurement machine (CMM). Body-fixed frames (dark grey) and inertial frames (light grey) for the IMU and end effector are also illustrated. The white dashed line denotes the rotational axis of the CMM's base and the solid white arrow denotes the position vector of the IMU relative to that axis.

numerically differentiated yielding an angular velocity signal to compare with that measured by the IMU, which allows for removing any time delay between their respective angular rates. The alignment movement is also used to determine the orientation between the IMU's sense axes and those of the body-fixed frame of the distal link in the CMM's kinematic chain (i.e., the link farthest from the base), hereafter referred to as the end effector. The $\hat{\boldsymbol{x}}_{CMM}$-axis is along the longitudinal axis of the end effector (aligned with the base axis in Fig. 3), the $\hat{\boldsymbol{y}}_{CMM}$-axis is collinear with the end effector's axis of rotation, and the $\hat{\boldsymbol{z}}_{CMM}$-axis is perpendicular to both.

A first calculation yields an intermediate estimate of the $\hat{\boldsymbol{z}}_{CMM}$-axis resolved in the IMU's body-fixed frame. The measured acceleration of the IMU during the alignment movement can be expressed as

$$\boldsymbol{a}_m = \dot{\boldsymbol{\omega}}_m \times \boldsymbol{r} + \boldsymbol{\omega}_m \times (\boldsymbol{\omega}_m \times \boldsymbol{r}) + \boldsymbol{g} \tag{30}$$

where $\boldsymbol{r}$ is the vector describing the position of the accelerometer embedded in the IMU relative to the vertical axis of rotation of the CMM and $\boldsymbol{g}$ is measured gravity. Since the base of the CMM only rotates about vertical, the acceleration

at the start of the alignment movement when the CMM is stationary is therefore $\boldsymbol{g}$. One then subtracts this measured value of $\boldsymbol{g}$ from Eqn. 30. Note that when the angular velocity achieves an extremum, the angular acceleration ($\dot{\boldsymbol{\omega}}_m$) is zero thereby circumventing the need for numerically differentiating the angular velocity data (and injecting another source of noise into the calculation). Evaluating Eqn. 30 (with $\boldsymbol{g}$ removed) at the extrema (say n times) results in n-equations

$$\begin{aligned} \boldsymbol{a}_{m,k} &= \boldsymbol{\omega}_{m,k} \times (\boldsymbol{\omega}_{m,k} \times \boldsymbol{r}) \\ &= (\boldsymbol{\omega}_{m,k}^{\times})^2 \boldsymbol{r} \\ &= \boldsymbol{\Omega}_{m,k} \boldsymbol{r} \end{aligned} \tag{31}$$

where k is the time step corresponding to the k^{th} extremum in the angular velocity. This produces an overdetermined, linear set of n equations that can be solved for $\boldsymbol{r}$ via

$$\boldsymbol{r} = \boldsymbol{A} / \boldsymbol{\Omega} \tag{32}$$

where $\boldsymbol{A}$ is a vector concatenating the accelerometer measurements, $\boldsymbol{\Omega}$ is a matrix concatenating the angular velocity measurements, and the backslash operator denotes the QR decomposition of the system of equations. Normalizing the resulting vector by its magnitude provides an intermediate estimate for the unit vector defining the direction from the IMU (accelerometer) to the CMM's vertical axis of rotation (i.e., the $\hat{\boldsymbol{z}}_{CMM}$-axis resolved in the IMU's body-fixed frame).

Next, a principal component analysis conducted on the angular velocity measured during the alignment movement provides as its first component the $\hat{\boldsymbol{x}}_{CMM}$-axis of the end effector of the CMM resolved in the IMU's body-fixed frame. One cross product ($\hat{\boldsymbol{z}}_{CMM} \times \hat{\boldsymbol{x}}_{CMM}$) yields the $\hat{\boldsymbol{y}}_{CMM}$-axis (which is normalized to be a unit vector) and a second cross product ($\hat{\boldsymbol{x}}_{CMM} \times \hat{\boldsymbol{y}}_{CMM}$) ensures the axes are orthonormal. Thus, the (constant) rotation matrix from the IMU frame to the CMM's end effector frame follows from

$$\boldsymbol{R}_{CMM/IMU} = \begin{bmatrix} \hat{\boldsymbol{x}}_{CMM} \\ \hat{\boldsymbol{y}}_{CMM} \\ \hat{\boldsymbol{z}}_{CMM} \end{bmatrix} \tag{33}$$

which (after being converted to a quaternion) pre-multiplies the quaternions estimated from the ESKF to relate the end-effector frame (not the IMU frame) to a world frame estimated by the IMUs.

Finally, the CMM's inertial frame differs, in general, from the world frame estimated by the IMUs. After the aforementioned pre-multiplication has been applied to the ESKF orientation estimates, the relationship between the CMM inertial frame and the IMU world frame is determined by comparing the initial end effector orientation provided by the ESKF method and the CMM at time 0. After post-multiplying the ESKF orientation estimates, the resulting (IMU-derived) ESKF estimates represent the orientation of the CMM end-effector relative to the CMM inertial frame.

Following the alignment movement, all rotational joints of the CMM are then unlocked allowing arbitrary three-dimensional rotations of the end effector for five consecutive trials. Each of the five trials lasts for approximately 5 minutes, which is ample time for very large orientation drift error to build if uncorrected. During this time, the CMM end effector is actuated by hand to induce large differences in orientation and with mean angular velocity and acceleration rates comparable to those observed for the foot during walking gait (8.3 rad/s and 53.1 m/s^2, respectively). Very brief pauses ($\leq$ 1 sec) during the data collection are also included to ensure the IMU remains still enough to correct for IMU orientation per the above method. Note that pauses, and even much longer pauses, are quite common and expected during human subject testing. For example, consider the pauses arising for the foot during the stance phase while walking. The source code for the algorithm described above has been made available on an open-source public web repository (https://github.com/rvitalium/ERKF).

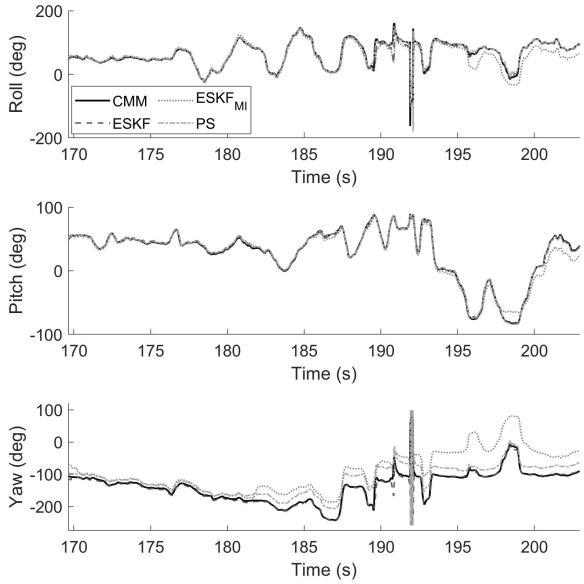

Fig. 4. Example results for roll, pitch, and yaw angles from the CMM (black) and IMU-derived estimates (grey curves) approximately halfway into one 5 minute trial. The IMU-estimates include those provided by the proprietary software (PS) and the above ESKF both with (ESKF) and without (ESKF_{MI}) considering magnetometer interference.

III. Results and Discussion

Figure 4 illustrates roll, pitch and yaw Euler angles for the IMU during a representative 30-second time interval from a five minute trial. The illustrated results provide a three-way comparison between the truth data (CMM) and three distinct estimates of the Euler angles from the IMU. Those estimates are provided by the proprietary software, and the above ESKF both with and without considering magnetometer interference (i.e., including or ignoring Criteria M1-3, respectively). Note that while all three IMU-derived estimates appear to track the truth data, the discrepancies generally increase with time as expected with drift error. In addition, the discrepancies in the yaw angle remain significantly larger than those for pitch and roll. This is also expected because the accelerometer data generally provides more reliable corrections to the pitch and roll estimates than the magnetometer data can provide reliable corrections to the yaw estimates. Overall, the discrepancies are

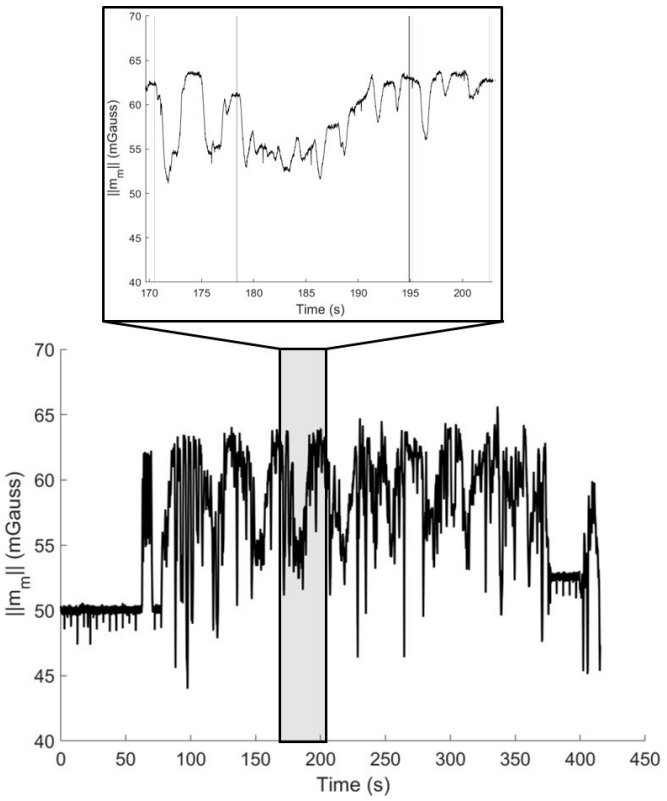

Fig. 5. Magnitude of the magnetic field during a sample 5-minute trial with an enlarged view of the same time period illustrated in Fig. 4. Grey regions in the enlarged view denote example time intervals when the magnetic field is approximately constant in satisfaction of Criterion M3 in the ESKF.

rather large for the ESKF without Criteria M1-3, are reduced for the proprietary software, and then are reduced again for the ESKF with Criteria M1-3. In fact, there is no perceptible difference between the truth data and the ESKF estimates using Criteria M1-3 on the scale of the plot in Fig. 4.

The RMS error between the true Euler angles and the estimated Euler angles provided by the ESKF that includes Criteria M1-3 for this trial (approximately 5 minutes) are 3.8°, 5.3°, and 5.9° for roll, pitch, and yaw, respectively. These errors also represent the largest of the five trials. Averaging across all five trials, the RMS errors are 3.4°, 3.5°, and 4.3° for roll, pitch, and yaw, respectively, which are comparable to other errors reported in the literature (see, for example, [18] or [37]). However, these results are significant in that they achieve comparable success in estimating IMU orientation over longer time periods. For example, the data collections in both [18] and [37] were limited to 2-minute trials compared to the substantially longer 5-minute trials herein.

These results also illustrate the effectiveness of the novel magnetometer criteria (Criterion M3) described previously (i.e., the time-invariant magnetic interference). Specifically, the RMS errors *without* Criterion M3 increase to 5.2°, 7.3°, and 7.9°, respectively, which represent an average 27% degradation. Figure 5 illustrates the magnitude of the magnetic field from the prior example trial with an enlarged view of the same time period considered in Fig. 4. Ideally, the magnetic field is constant. However, the large and observable fluctuations demonstrate the challenge of using the magnetometer data to correct for integration drift error about vertical. In this case, the magnetic interference likely derives from the CMM as the on-board electronics and ferromagnetic materials perturb the local magnetic field of the laboratory. Clearly, such large fluctuations in the magnetic field preclude using the magnetometer data for reliable estimates of magnetic North and for the majority of the trial. However, the grey shaded areas (see enlarged view) denote instances when the magnetometer data is approximately constant and since they are approximately constant (albeit over small time intervals), they can then be used to correct the estimated states per the ESKF above. Consequently, the robust ESKF yields excellent estimates of orientation despite the large fluctuations in the magnetic field; refer to Fig. 5.

TABLE I
QUANTITATIVE COMPARISONS OF EULER ANGLES ACROSS ALL FIVE TRIALS, INCLUDING RMS ERROR, CORRELATION (r), AND SLOPE, AND Y-INTERCEPT (b) OF LINEAR FIT

	RMS Error (°)	r	Slope	b (°)
Roll	3.4	0.99	1.00	-0.77
Pitch	3.5	0.99	0.99	0.13
Yaw	4.3	0.99	1.00	-0.07

TABLE II
QUANTITATIVE COMPARISONS OF EULER ANGLES ACROSS ALL FIVE TRIALS USING ESKF ESTIMATES WITHOUT CONSIDERATION FOR MAGNETOMETER INTERFERENCE AND THE PROPRIETARY ESTIMATES

	Mag. Interference Ignored		Proprietary Software	
	RMS Error (°)	r	RMS Error (°)	r
Roll	12.7	0.99	8.30	0.99
Pitch	10.7	0.99	6.54	0.99
Yaw	14.9	0.95	26.7	0.94

Finally, we analyze the agreement between the Euler angles estimated by the ESKF (that considers magnetic field interference) and the truth (CMM) data. Table I reports the resulting best fit lines and correlation coefficients across all five trials (cumulatively 25 minutes). Overall, the IMU estimates exhibit excellent correlation with the truth data.

By contrast, Table II reports the RMS errors and correlation coefficients for the other comparisons previously considered; namely, between truth data and the output of the proprietary software and the ESKF that does not consider magnetic interference (i.e., ignores Criterion M1-3). While the degradation in the correlation coefficients for both of these latter comparisons is relatively small, the overall RMS error (across all five trials) grows considerably and most notably for the yaw estimates. These results highlight the importance of estimation methods that remain robust in the presence of imperfect measurements of magnetic North and vertical (gravity).

IV. CONCLUSION

This study contributes a robust Error-State Kalman Filter (ESKF) for estimating IMU orientations that yields highly accurate results when benchmarked on a coordinate measurement machine (CMM). The ESKF remains robust to poor measurement updates for magnetic north and/or gravity

(vertical). Consequently, accurate orientation estimates result even in environments when the magnetic field experiences large fluctuations or when the IMU is subject to highly dynamic movements. Results demonstrate that the ESKF yields highly accurate results for three-dimensional rotations (as measured by three Euler angles) when compared to truth data from the CMM. In particular, the Euler angles closely replicate the truth data (with RMS errors below 3.7°) even in the presence of large fluctuations in the magnetic field. In parallel, the agreement between the IMU-estimated orientations and the orientations provided by the CMM is excellent, thus providing support for this estimation method.

REFERENCES

[1] R. Vitali *et al.*, "Method for estimating three-dimensional knee rotations using two inertial measurement units: Validation with a coordinate measurement machine," *Sensors*, vol. 17, no. 9, p. 1970, Aug. 2017.

[2] E. R. Bachmann, R. B. McGhee, X. Yun, and M. J. Zyda, "Inertial and magnetic posture tracking for inserting humans into networked virtual environments," in *Proc. ACM Symp. Virtual Reality Softw. Technol. (VRST)*, 2001, pp. 9–16.

[3] R. Mahony, T. Hamel, and J.-M. Pflimlin, "Nonlinear complementary filters on the special orthogonal group," *IEEE Trans. Autom. Control*, vol. 53, no. 5, pp. 1203–1218, Jun. 2008.

[4] S. O. H. Madgwick, A. J. L. Harrison, and R. Vaidyanathan, "Estimation of IMU and MARG orientation using a gradient descent algorithm," in *Proc. IEEE Int. Conf. Rehabil. Robot.*, Zürich, Switzerland, Jun. 2011, pp. 1–7.

[5] K. Feng *et al.*, "A new quaternion-based Kalman filter for real-time attitude estimation using the two-step geometrically-intuitive correction algorithm," *Sensors*, vol. 17, no. 9, p. 2146, Sep. 2017.

[6] R. McGinnis, S. Cain, S. Davidson, R. Vitali, S. McLean, and N. Perkins, "Validation of complementary filter based IMU data fusion for tracking torso angle and rifle orientation," in *Proc. ASME Int. Mech. Eng. Congr. Expo.*, 2014, pp. 1–10.

[7] M. Kok and T. B. Schon, "A fast and robust algorithm for orientation estimation using inertial sensors," *IEEE Signal Process. Lett.*, vol. 26, no. 11, pp. 1673–1677, Nov. 2019.

[8] J. Wu, Z. Zhou, H. Fourati, R. Li, and M. Liu, "Generalized linear quaternion complementary filter for attitude estimation from multisensor observations: An optimization approach," *IEEE Trans. Autom. Sci. Eng.*, vol. 16, no. 3, pp. 1330–1343, Jul. 2019.

[9] K. A. Strausser and H. Kazerooni, "The development and testing of a human machine interface for a mobile medical exoskeleton," in *Proc. IEEE/RSJ Int. Conf. Intell. Robots Syst.*, Sep. 2011, pp. 4911–4916.

[10] S. Wilson *et al.*, "Formulation of a new gradient descent MARG orientation algorithm: Case study on robot teleoperation," *Mech. Syst. Signal Process.*, vol. 130, pp. 183–200, Sep. 2019.

[11] A. Fung, E. C. Lai, and B.-C. Lee, "Usability and validation of the smarter balance system: An unsupervised dynamic balance exercises system for individuals with Parkinson's disease," *IEEE Trans. Neural Syst. Rehabil. Eng.*, vol. 26, no. 4, pp. 798–806, Apr. 2018.

[12] M. Raitoharju and R. Piché, "On computational complexity reduction methods for Kalman filter extensions," 2015, *arXiv:1512.03077*. [Online]. Available: http://arxiv.org/abs/1512.03077

[13] R. Zhu and Z. Zhou, "A real-time articulated human motion tracking using tri-axis inertial/magnetic sensors package," *IEEE Trans. Neural Syst. Rehabil. Eng.*, vol. 12, no. 2, pp. 295–302, Jun. 2004.

[14] A. L. C. Quigley, "An approach to the control of divergence in Kalman filter algorithms," *Int. J. Control*, vol. 17, no. 4, pp. 741–746, Apr. 1973.

[15] V. Madyastha, V. Ravindra, S. Mallikarjunan, and A. Goyal, "Extended Kalman filter vs. error state Kalman filter for aircraft attitude estimation," in *Proc. AIAA Guid., Navigat., Control Conf.*, Portland, OR, USA, Aug. 2011, pp. 1–23.

[16] N. Yadav and C. Bleakley, "Accurate orientation estimation using AHRS under conditions of magnetic distortion," *Sensors*, vol. 14, no. 11, pp. 20008–20024, Oct. 2014.

[17] S. Habbachi, M. Sayadi, and N. Rezzoug, "Partical filtering for orientation determining using inertial sensors IMU," in *Proc. 4th Int. Conf. Adv. Technol. Signal Image Process. (ATSIP)*, Sousse, Tunisia, Mar. 2018, pp. 1–5.

[18] A. M. Sabatini, "Quaternion-based extended Kalman filter for determining orientation by inertial and magnetic sensing," *IEEE Trans. Biomed. Eng.*, vol. 53, no. 7, pp. 1346–1356, Jul. 2006.

[19] Á. Odry, I. Kecskes, P. Sarcevic, Z. Vizvari, A. Toth, and P. Odry, "A novel fuzzy-adaptive extended Kalman filter for real-time attitude estimation of mobile robots," *Sensors*, vol. 20, no. 3, p. 803, Feb. 2020.

[20] S. J. Julier and J. K. Uhlmann, "New extension of the Kalman filter to nonlinear systems," *Proc. SPIE*, vol. 3068, pp. 182–193, Apr. 1997.

[21] S. Cardarelli *et al.*, "UKF magnetometer-free sensor fusion for pelvis pose estimation during treadmill walking," in *Proc. 41st Annu. Int. Conf. IEEE Eng. Med. Biol. Soc. (EMBC)*, Jul. 2019, pp. 1213–1216.

[22] A. Barrau and S. Bonnabel, "Invariant Kalman filtering," *Annu. Rev. Control, Robot., Auton. Syst.*, vol. 1, pp. 237–257, May 2018.

[23] R. Hartley, M. Ghaffari, R. M. Eustice, and J. W. Grizzle, "Contact-aided invariant extended Kalman filtering for robot state estimation," *Int. J. Robot. Res.*, vol. 39, no. 4, pp. 402–430, Mar. 2020.

[24] S. I. Roumeliotis, G. S. Sukhatme, and G. A. Bekey, "Circumventing dynamic modeling: Evaluation of the error-state Kalman filter applied to mobile robot localization," in *Proc. IEEE Int. Conf. Robot. Automat.*, Detroit, MI, USA, May 1999, pp. 1656–1663.

[25] J. Solà, "Quaternion kinematics for the error-state Kalman filter," *CoRR*, pp. 1–95, Nov. 2017. [Online]. Available: http://arxiv.org/abs/1711.02508

[26] D. Gebre-Egziabher, G. Elkaim, J. Powell, and B. Parkinson, "A non-linear, two-step estimation algorithm for calibrating solid-state strap-down magnetometers," in *Proc. Int. Conf. Navigat. Syst.*, St. Petersburg, Russia, May 2001, pp. 28–30.

[27] Y. Xu, J. Quo, and Y. Guan, "EKF based multiple-mode attitude estimator for quadrotor using inertial measurement unit," in *Proc. 36th Chin. Control Conf. (CCC)*, Jul. 2017, pp. 6191–6198.

[28] X. Xu, X. Tian, L. Zhou, and Y. Li, "A decision-tree based multiple-model UKF for attitude estimation using low-cost MEMS MARG sensor arrays," *Measurement*, vol. 135, pp. 355–367, Mar. 2019.

[29] C. W. Kang and C. G. Park, "Attitude estimation with accelerometers and gyros using fuzzy tuned Kalman filter," in *Proc. Eur. Control Conf. (ECC)*, Aug. 2009, pp. 3713–3718.

[30] D. Roetenberg, H. J. Luinge, C. T. M. Baten, and P. H. Veltink, "Compensation of magnetic disturbances improves inertial and magnetic sensing of human body segment orientation," *IEEE Trans. Neural Syst. Rehabil. Eng.*, vol. 13, no. 3, pp. 395–405, Sep. 2005.

[31] H. Luinge, D. Roetenberg, and P. Slycke, "Motion tracking system," U.S. Patent 8 165 844, Apr. 24, 2012.

[32] A. Vydhyanathan and G. Bellusci, "The next generation xsens motion trackers for industrial applications," Xsens, Enschede, The Netherlands, White Paper, 2015.

[33] J. Wu, "Real-time magnetometer disturbance estimation via online nonlinear programming," *IEEE Sensors J.*, vol. 19, no. 12, pp. 4405–4411, Jun. 2019.

[34] N. Trawny and S. Roumeliotis, "Indirect Kalman filter for 3D attitude estimation," Dept. Comput. Sci. Eng., Univ. Minnesota, Minneapolis, MN, USA, Tech. Rep. 2005-002, 2005.

[35] P. C. Mahalanobis, "On the generalized distance in statistics," in *Proc. Nat. Inst. Sci. India*, vol. 2, no. 1, pp. 49–55, 1936.

[36] N. K. Shah and P. J. Gemperline, "Combination of the Mahalanobis distance and residual variance pattern recognition techniques for classification of near-infrared reflectance spectra," *Anal. Chem.*, vol. 62, no. 5, pp. 465–470, Mar. 1990.

[37] A. Brennan, J. Zhang, K. Deluzio, and Q. Li, "Quantification of inertial sensor-based 3D joint angle measurement accuracy using an instrumented gimbal," *Gait Posture*, vol. 34, no. 3, pp. 320–323, Jul. 2011.